applied sciences

MDPI

Article

Application of Classified Elastic Waves for AE Source Localization Based on Self-Organizing Map

Katsuya Nakamura *, Yoshikazu Kobayashi *, Kenichi Oda and Satoshi Shigemura

Department of Civil Engineering, College of Science and Technology, Nihon University, Tokyo 101-8308, Japan; oda.kenichi@nihon-u.ac.jp (K.O.); shigemura.satoshi@nihon-u.ac.jp (S.S.)

* Correspondence: nakamura.katsuya@nihon-u.ac.jp (K.N.); kobayashi.yoshikazu@nihon-u.ac.jp (Y.K.)

Abstract: Acoustic emission (AE) source localization has been used to visualize progress failures generated in a wide variety of materials. In the conventional approaches, AE source localization algorithms assume that the AE signal is propagated as a straight line. However, it is supposed that progress failures form heterogeneity of elastic wave velocity distributions. Hence, with the conventional source localization, it is expected that the localization accuracy is reduced in heterogeneous materials since diffraction and refraction waves are generated. Thus, if the straight propagation waves are classified, conventional source localizations are performed in the heterogeneous materials. The self-organizing map (SOM) is one of the unsupervised learning methods, and the SOM has potential to classify straight propagation waves for the source localizations. However, the application of classified AE signals in source localization is not popular. If classified AE signals are applied to the time difference of arrival (TDOA) method, which is the popular localization method, it is expected that number of visualized sources are decreased because the algorithm does not consider the selection of the propagated wave. Although ray tracing has potential to localize a larger number of sources than the TDOA method, it is expected that the localized sources are less accurate in comparison with results of the TDOA method. In this study, classified waves were applied to two of the source localizations, and model tests based on pencil-lead breaks (PLBs) generating artificial AE sources were conducted to validate the performance of the source localizations with classified waves. The results of the validation confirmed that the maximum error in the TDOA method is larger in comparison with ray tracing conducted with 20 mm intervals of source candidates. Moreover, ray tracing localizes the same number of sources as the number of PLB tests. Therefore, ray tracing is expected to more practically localize AE sources than the TDOA method if classified waves are applied.

Keywords: AE source localization; heterogeneous materials; self-organizing map; unsupervised learning methods

Citation: Nakamura, K.; Kobayashi, Y.; Oda, K.; Shigemura, S. Application of Classified Elastic Waves for AE Source Localization Based on Self-Organizing Map. *Appl. Sci.* **2023**, *13*, 5745. https://doi.org/10.3390/app13095745

Academic Editor: Giuseppe Lacidogna

Received: 9 April 2023
Revised: 2 May 2023
Accepted: 5 May 2023
Published: 6 May 2023

1. Introduction

Acoustic emissions (AEs) are elastic waves occurring with micro-cracks and/or frictions, and they have been applied to non-destructive testing (NDT) [1–4]. In particular, AE source localization has potential to detail the progress failures in materials. In the field of geotechnical engineering, AE sources generated by triaxial compression tests have visualized shear bands developed in saturated sand [5]. Moreover, source localization has been applied to the visualization of particle breakages during pile penetration in the soil tank [6]. Furthermore, source localization has visualized micro-cracks that appeared in infrastructures [7,8], and it has been used in the field of health monitoring of existing structures.

The time difference of arrival (TDOA) method [9] is one of the source localization methods. Owing to the straight propagations assumed in the algorithm of the TDOA method, the lengths of the ray paths from the source to the sensors and the arrival time difference in combinations of sensor locations can be used in defining the equation for the source localization. Furthermore, arrival times of AE signals are detected from measured

time-history waveforms, and the detected arrival times are used for the input data of the TDOA method. Thus, the TDOA method has applicability since the TDOA method can localize sources generated in various materials if the AE signals can be measured at each sensor. In addition, it has been widely used in the field of NDT [5,6,10] because of the above applicability.

The elastic wave velocity distributions of specimens used in element or model tests are expected to be updated by loading; for instance, the heterogeneous velocity distributions of the rock materials in triaxial tests are identified [11]. However, diffraction and refraction waves are generated in the heterogeneities of the velocity distributions, and it is difficult for the TDOA method to be conducted with element or model tests if velocity distributions are updated. Moreover, progress failures possibly form the heterogeneity in existing structures and are expected to decrease the accuracy of health monitoring based on the TDOA method. In recent approaches, Dong et al. identified a defects area, and the AE source localization was conducted with the considered defects area [12]. Furthermore, Jones et al. applied Gaussian process regression to Bayesian source localization to localize sources generated in complex structures [13]. Furthermore, these approaches use elastic wave arrival times in which the input data are the same as in the TDOA method. Since huge numbers of AEs are generated in AE measurements [14,15], the arrival time is generally detected by automatic picking algorithms. In automatic picking algorithms, the uses of characteristic functions have been applied to measured waveforms, and the time wherein the value of the functions exceeds the threshold has been defined as the wave arrival time [16,17]. In addition, the Akaike information criterion (AIC) has been used for arrival-time detections conducted in measured waveforms [18,19], and AIC pickers do not require the use of the threshold considered for the measurement conditions in the arrival-time detection since the arrival times are defined as evaluated boundaries between noises and signals. Although these automatic picking algorithms can detect accurate arrival times from high S/N signals, it is supposed that the accuracy of arrival-time detections is decreased in low S/N signals since the index of arrival times is computed from amplitude differences in the waveform. According to the Huygens–Fresnel principle, the amplitude is attenuated with an angle of the diffraction. Thus, it implies that the accuracy of an arrival time detected from a diffraction wave is decreased, and it is then challenging for an arrival time detected from a diffraction wave to be applied to source localizations.

If straight propagation waves are classified from measured waveforms, AE source localizations do not require consideration of the diffraction and refraction waves. The self-organizing map (SOM) [20] is one of the unsupervised learning methods, and relations of measured data are visualized. In the previous study, classified artificial AE signals by the SOM were used in the source localizations based on ray tracing [21] and improved the accuracy of localized sources generated in the heterogeneous velocity distributions [22]. However, the source localizations based on ray tracing select candidates of AE sources, wherein they are set in an analytical model. Since the TDOA method does not require the use of the candidates, it is expected that the TDOA method localizes sources more accurately in comparison with the application of ray tracing in the use of straight propagation. In the use of classified waves, used sensors which measure straight propagations are selected, and it is implied that the number and the location of used sensors are not same as each localization. It is expected that the limited sensors contribute to a divergence of the computation in the TDOA method, and the application of ray tracing localizes a larger number of sources than results of the TDOA method. In this study, classified waves were applied to two of the source localizations, which are the TDOA method and the application of ray tracing, and the model tests based on pencil-lead breaks (PLBs), which are widely used in the study of the source localization to generate artificial AE sources [23–26], were conducted to validate the performance of the source localizations with classified waves. Furthermore, the results of the validation discuss the localization accuracy, the number of visualized sources to evaluate, and which method is preferred for applying to classified waves. Moreover, results of the SOM rely on a selection of the used data, and it is supposed

that the classification accuracy depends on the AE signals used in the SOM. Thus, the selection of the used AEs in the SOM is validated to evaluate the localization accuracy.

2. AE Source Localization

Although the accuracy of the TDOA method can possibly be improved by the classified waves, the divergence of the TDOA algorithm is expected to occur because of the application of classified waves. In addition, it is supposed that the accuracy of ray tracing depends on the interval of the candidates. These factors are detailed in Sections 2.1 and 2.2.

2.1. TDOA Method

The source localized by the TDOA method is illustrated in Figure 1. In the TDOA algorithm, the equations of the source localization are obtained as

$$R_i - R_j = (A_i - A_j)v_p, \tag{1}$$

where R_i and R_j are the lengths of the ray paths from the localized source to sensors i and j; A_i and A_j are the arrival times at ith and jth sensors; and v_p is a propagation velocity. Moreover, R_i is defined as

$$R_i = \|r_i - r_o\|_2, \tag{2}$$

where r_i and r_o are the position vectors of the ith sensor and the source o. It is noted that the components of r_o are the variables. In Equation (1), v_p is assumed to be homogeneous in the model because the ray path is defined as the straight line. Therefore, the TDOA method requires classifying the straight lines from measured waves to consider the diffraction and the refraction waves if the sources are localized in the heterogeneity.

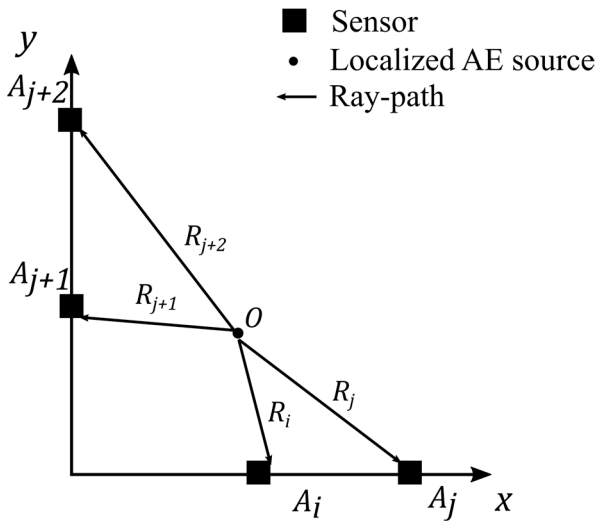

Figure 1. The illustration of the TDOA method.

The numbers of Equation (1) are determined by subtracting one from the number of sensors. Although Equation (1) requires two equations in the two dimensions, the several sensors should be applied to the heterogeneous velocity distributions because used sensors are selected by classified waves. Thus, it implies that the number of equations is larger in comparison with the number of the variables. In order to compute the large number of equations, the least squares method is applied. However, the particular locations of the sensors used in Equation (1) have potential to obtain a determinant of 0 if the used sensors are only located in an axis. Therefore, it is possible that the TDOA method does not localize the source in the application of the classification.

2.2. Use of Ray Tracing for the Source Localization

In the source localization using ray tracing, the source is localized on the basis of first travel times of approximated ray paths. Although ray tracing performs the approximation of ray paths considering the diffraction or the refraction, ray tracing requires an analytical model to approximate the heterogeneity of the materials. If the classified waves are applied to the source localization using ray tracing, the localization does not require approximating the heterogeneity of the materials to compute the first travel times of approximated ray paths since classified waves consist of straight propagation.

In order to detail the source localization, the illustration of the localization is shown in Figure 2. Moreover, the possible pulse-origination time P_{ij} is defined by subtracting the first travel time from the arrival time, obtained as

$$P_{ij} = A_i - Tr_{ij}, \tag{3}$$

where Tr_{ij} is travel time of the wave, wherein the start is the sensor i and the end is the candidate j. The AE source is selected from the candidates, and the index of the selected candidate is the minimum variance of the origination time σ_j^2, obtained as

$$\sigma_j^2 = \frac{1}{N_s}\sum_{i=1}^{N_s}\left(\bar{P}_j - P_{ij}\right)^2, \tag{4}$$

where N_s is the number of used sensors, and $\bar{P}_j$ is the average of P_{ij}. It is noted that the computation of σ_j^2 is not required of all located sensors in the model, and it implies that the used sensors in the source localization can be selected by the result of classifications. Moreover, although the particular location of the sensors contributes to the determinant of 0 in computation of the TDOA method, the application of ray tracing has potential to localize all of the sources since the computation of matrix equations is not required. However, the interval of candidates contributes to the accuracy of the localization because the candidate is selected as the AE source. Thus, it is possible that the accuracy of the source localization based on ray tracing is lower in comparison with the TDOA method if the interval of the candidates is not sufficient in the model. Furthermore, decreasing the interval of candidates contributes to increasing computational time because the numbers of the candidates are increased in the models.

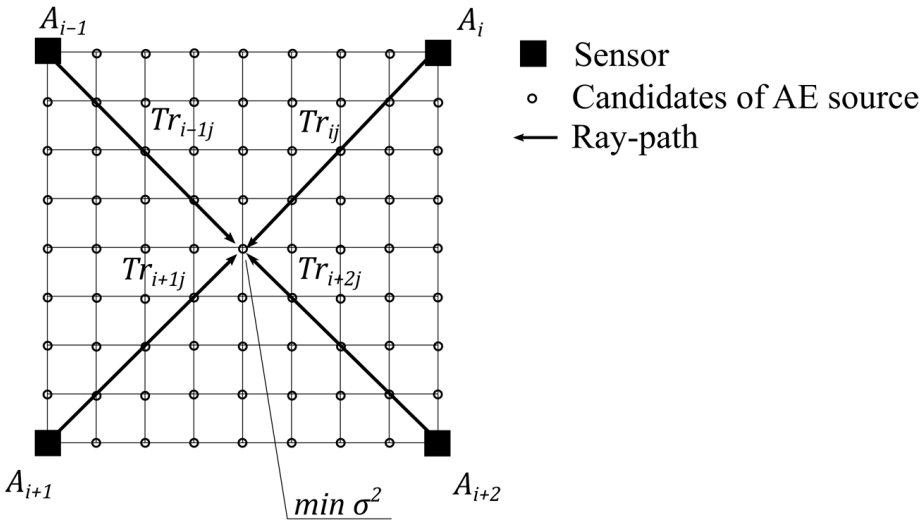

Figure 2. Illustration of the localization using ray tracing.

3. Application of the SOM

In Sections 3.1 and 3.2, the architecture of the used SOM and a process of the classification are detailed. It is noted that this application of the SOM refers to the previous study [22]. Moreover, two of the localizations considering homogeneous elastic waves are conducted with arrival times detected from the classified waves.

3.1. Architecture of the SOM

In the illustration of the SOM shown in Figure 3, the neurons that had the weight vectors are set in an output layer and the class is visualized by the neurons. Firstly, the weight vectors have random values and are iteratively updated by the input vectors. Moreover, updates of the weight vectors are conducted on the basis of the winning neuron M_c, and M_c is chosen as

$$\|X_i - M_c\|_2 = \min_{0 \le j < N} \|X_i - M_j\|_2, \tag{5}$$

where X_i is the ith input vector, the weight vector M_j is in the neuron j, and N is number of neurons. Moreover, x is the input vector component, m is the weight vector component, and X_i and M_j have the number of vector components n. According to Equation (5), M_c is selected in combinations of all of neurons. Furthermore, the neighbors of M_c are updated by Equation (6), obtained as

$$M_j' = M_j + h_c[X_i - M_j], \tag{6}$$

where M_j' is the updated weight vector in the neuron j, and h_c is the neighborhood function. It is noted that M_j' is computed on the basis of h_c, and h_c is obtained as

$$h_c = a(k) exp\left(-\frac{\|r_c - r_j\|_2^2}{2\sigma^2(k)}\right), \tag{7}$$

where $a(k)$ and $\sigma(k)$ are monotonically decreasing functions, and r_c and r_j are the position vectors of M_c and M_j. Moreover, the initial value of $a(k)$ is 1.0, and the initial value of $\sigma(k)$ implies the initial radius of the update. In order to protect the diverges in the computation of classes, the values and the targets of h_c are required to decrease with the iterations. Hence, the outputs of $a(k)$ and $\sigma(k)$ are, respectively, reduced with the iteration count of k. Furthermore, the maximum value of h_c is computed if r_j is equal to r_c and decreases with the distance between r_j and r_c. It is worth noting that since the neurons are updated using h_c, the group of neurons that had similarity to the vectors appears around M_c, and the group of neurons implies the classes in the SOM algorithm. Furthermore, Equations (5)–(7) are iteratively conducted with all of X_i. Thus, M_c is obtained by each X_i, and each class is formed by several M_c. Moreover, the large iteration contributes to expansion of the class, and it is supposed that the size of class in the map depends on the number of M_c. It should be noted that the iteration count of k is increased if all of X_i is applied to Equations (5)–(7). Furthermore, the class considers the dispersion of the data since Equation (7) to be defined as the Gaussian function. Therefore, it is implied that the SOM has the ability to form the class with limited data because the weight vectors in the class are interpolated by Equation (7).

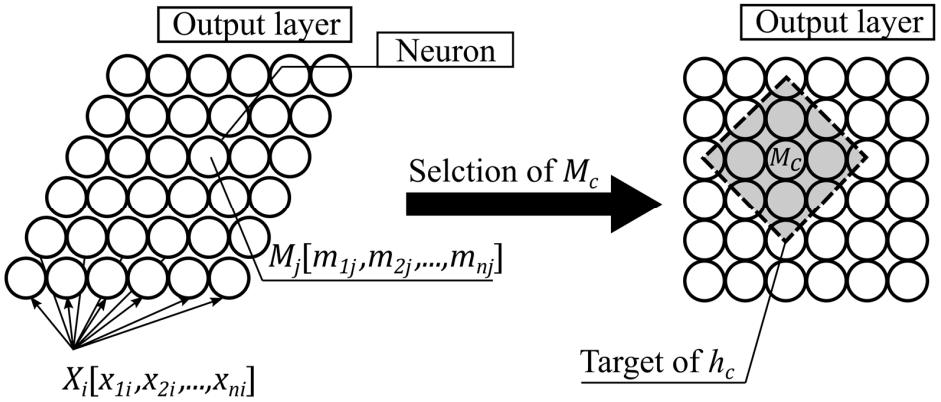

Figure 3. The conceptual diagram of SOM.

3.2. Classification of the Waves

The map defined as the output layer can be used in the classification because the class of M_c implies the class of the data if M_c in the map is chosen by the data. Therefore, if the SOM forms a high S/N class, wherein neurons are updated by high S/N signals, it is supposed that the computed class choses the waves used in AE source localizations.

The number of vector components implies the characteristics of the measured data. Moreover, since a large number of the characteristics increase the number of classes, the classes are possibly scattered in the map. Furthermore, scattered classes are expected to have identical data classified in different classes. Therefore, the input vector components should be decreased. In order to reduce the input vector components used in this classification, the components are defined as the root-mean-square voltage computed in the equally divided waveform. To illustrate the computation of the components, the divided waveform is shown in Figure 4, and the root-mean-square voltage V_i is obtained as

$$V_i = \sqrt{\frac{1}{T_i}\int_0^{T_i} y^2(t)dt}, \tag{8}$$

where T_i is the duration time in the ith divided waveform, $y(t)$ is the divided waveform, and t is the time. In Figure 4, the waveform is divided into three parts, and it implies that the number of components is three in this SOM analysis. It is supposed that three components are enough for the formation of the class since the SOM has been conducted with RGB values, which are defined as three-dimensional vectors [27].

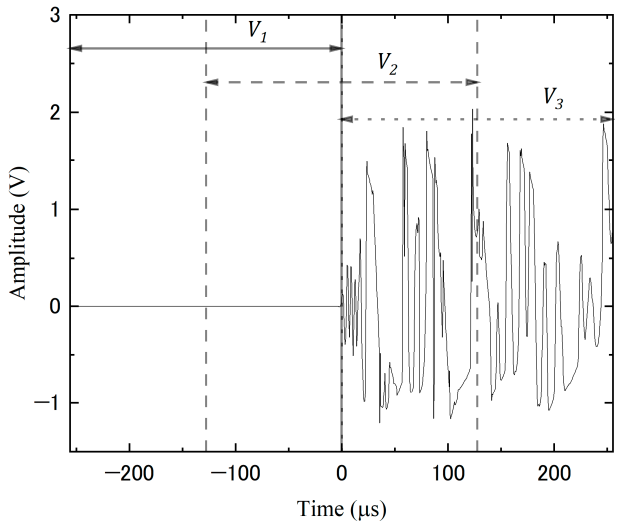

Figure 4. Example of the waveform divided for computation of the input vector components.

To define borders of the classes, the computation of similarity in the weight vectors, for instance, by the K-means algorithm, was applied [28]. In this study, three types of classes, namely, the high S/N, low S/N, and noise classes, are assumed in the measured waves, and the three representative weight vectors in each class are selected to define the border as the minimum Euclidean distance from the neurons to the representative weight vectors. If the representative weight vectors are used for the criterions, the computation of the similarity does not require the same iteration as the K-means algorithm. In the heterogeneous models, the diffraction and refraction waves are generated, and these amplitudes are lower in comparison with the straight waves because of the diffraction and refraction attenuations. Hence, it is expected that the straight waves are the high S/N class, and the diffraction and refraction waves are the low S/N class. Moreover, the noises are assumed to be lower amplitudes than the measured signals, and the noise classes contributed to the classification of noises in the previous study [22]. In Figure 4, a ration of V_3 to V_1 implies levels of S/N in the measured waveforms because 0 μs is start of the measurement, and high S/N signals generally start from 0 μs. Furthermore, the level of S/N L_V is obtained as

$$L_V = 20\log \frac{V_3}{V_1}. \tag{9}$$

Hence, in the obtained map, it is supposed that the neuron that has the highest L_V belongs to the high S/N class, and the noise class includes the neuron that has the lowest L_V. Therefore, the representative weight vectors allocated in the neurons wherein the highest and the lowest L_V are computed are expected to be used for the criterions defining the high S/N class and the noise class. Furthermore, the criterion of the low S/N class is the average vectors computed by other criterions since the amplitudes of the low S/N are assumed to be larger than the amplitudes of noises.

4. Experimental Set Up

In this model test, the artificial AEs are generated at PLB points, and the localization accuracy is evaluated by the differences between sources localized by the use of measured artificial AEs and locations of PLB points. In Section 4.1, the size of a used specimen and the measurement conditions of artificial AEs are detailed. It should be noted that a defect is applied to the metal material used for the specimen to set a heterogeneous velocity distribution. In Section 4.2, the locations of PLB points and sensors are shown to detail the conditions of the localizations and the SOM.

4.1. Specimen of Model Test and Artificial AE Measurement Flow

A used aluminum plate and installed sensors are shown in Figure 5. The aluminum plate is formed square-shaped, which is a size of 1000 mm and a thickness of 5.0 mm. Furthermore, the defect located at 730 mm from the upper of the specimen is a height of 40 mm and width of 500 mm. Furthermore, the notations of the sensors are S1–S12. If an AE is generated in the specimen, the diffraction wave is propagated around the defect. Moreover, a large number of diffraction waves are acquired at S3 and S4 since the defects are located in bottom right. Although huge localization errors are expected to appear in the source localizations considering the homogeneous model, the classified waves are expected to consist of direct propagation, improving the accuracy of localization in the specimen.

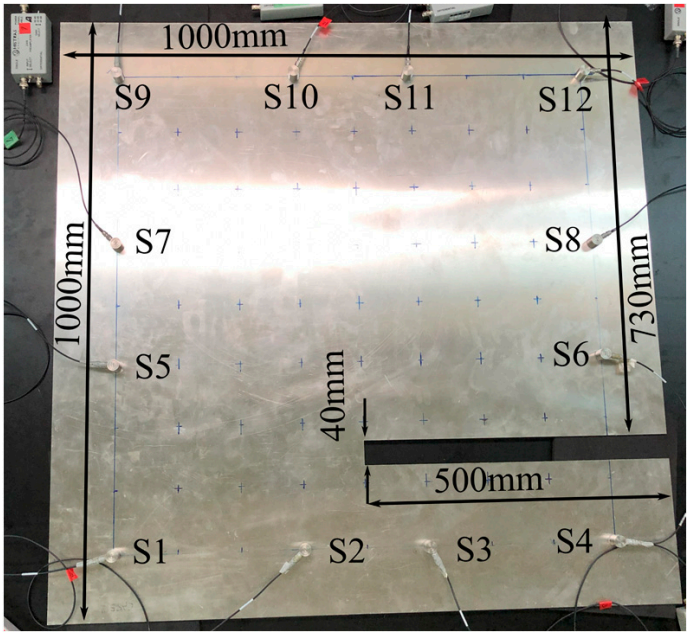

Figure 5. The aluminum plate used as the specimen.

These measurement conditions refer to the previous study [29] in which a PLB test was conducted in an aluminum plate. A flow of artificial AE measurement is illustrated in Figure 6. In the model test, artificial AEs generated by PLBs are acquired by the resonant sensors, wherein the resonant frequency is 55 kHz. Moreover, acquired signals are amplified 40 dB in the preamp and amplified signals are measured with the sampling rate 2 MHz in the used measurement board. It should be noted that the installed sensors, preamps, and measurement board are produced by PAC [30]. In the system produced by PAC, the waveform is acquired when an amplitude exceeds the measurement trigger, and the arrival time used in the source localizations is detected from the waveform. In this study, AR-AIC [18] is conducted in the waveforms measured by the measurement trigger 55 dB. An example of the detection is shown in Figure 7. In the AR-AIC algorithm, the autoregressive model is used to evaluate the start of the signals by the minimum AIC value. In addition, AR-AIC has been applied to a source localization considered homogeneous [6], and it is supposed that the detected arrival times are sufficiently accurate for the source localizations if only the straight propagation waves are used.

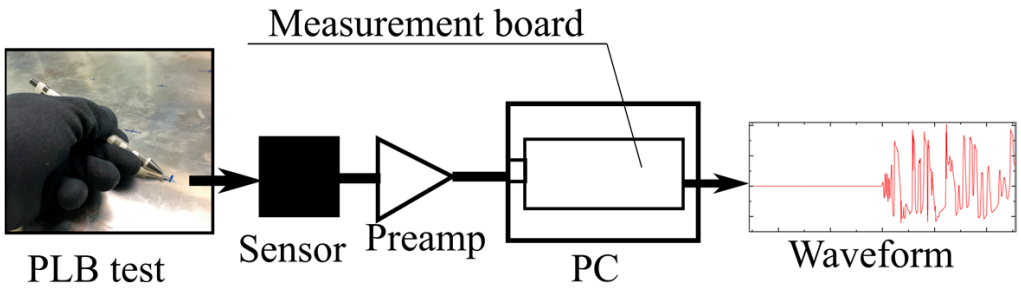

Figure 6. Artificial AE measurement flow.

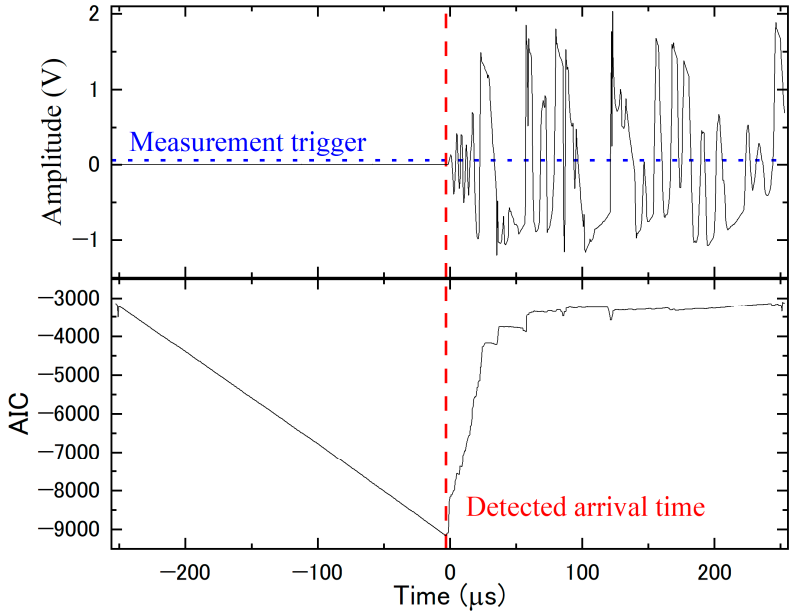

Figure 7. Illustration of measurement trigger and detected arrival time by AR-AIC.

4.2. Location of the Generated Sources and Sensors

In the PLB tests, the used pencil leads were 0.5 mm and 2 H in diameter and hardness, respectively. Moreover, the locations of the PLB tests are shown in Figure 8. In Figure 8, white dots imply the sources generated by PLB tests located with intervals of 100 mm. Thus, the number of total PLB points is 49, and it is expected that 49 sources are localized. The localized sources are shown in the xy orthogonal coordinate system, and the original point is defined as S1. In the orthogonal coordinate system, the locations of sensors are listed in Table 1. The analytic model is defined as the rectangle consisting of the vertexes, which are S1, S4, S9, and S12. Although the number of sensors should be increased for greater accuracy of the source localizations, the computational costs of the SOM are increased with a large number of input vectors for the classification of elastic waves. Owing to the conservation of computational costs, the selection of sensors is required. Furthermore, if the number of classes of input vectors has a bias, it is expected that having several input vectors does not contribute to the visualization of classes since the map is updated on the basis of input vectors computed from waveforms. If diffraction waves are measured in the limited sensors, since a defect is local in a specimen, the number of diffraction waves is particularly smaller in comparison with all of the measured waves. It is challenging that a small number of diffraction waves forms the class wherein diffraction waves belong. Therefore, the measured waves should be selected to be applied to the SOM. In this model test, the SOM is conducted with artificial AE signals measured at the sensors located in the vertexes of the rectangle shown in Figure 8. Although the locations of diffraction waves arrivals are unknown because identifying locations of failures generated inside of structures is challenging, it is expected that the sensors located in the vertexes can measure diffraction waves if the model is defined as a rectangle. Furthermore, the appropriate number of straight propagation waves are expected to be applied to the input vectors because the number of straight propagation waves is decreased in waves used in the SOM. Hence, measured waves at all of the vertexes have potential to form the class wherein diffraction waves belong.

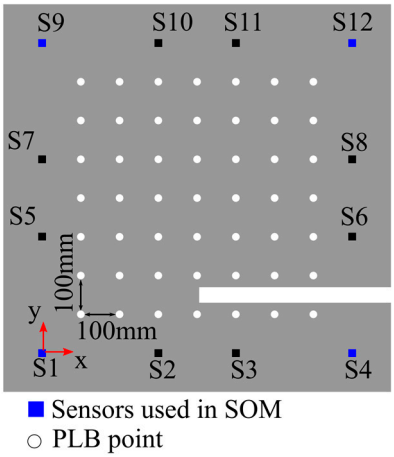

Figure 8. Locations of PLB points and sensors.

Table 1. Locations of installed sensors in the specimen.

Sensors	x (mm)	y (mm)
S1	0	0
S2	300	0
S3	500	0
S4	800	0
S5	0	300
S6	800	300
S7	0	500
S8	800	500
S9	0	800
S10	300	800
S11	500	800
S12	800	800

5. Results

5.1. Results of the Classification

In the map shown in Figure 9, the cells imply that the neurons and the center of the cell set to three dimensions of the vectors had the components computed by the root-mean-square voltages. The number of input vectors is 214, the same as the number of the waves measured at S1, S4, S9, and S12. Furthermore, the map consists of 64 neurons, and the number of the neurons is obtained by the use of the heuristic equation applied to an application of the SOM [31]. In Figure 9, the neurons visualize three classes formed by the similarities of the vectors detailed in the Section 3.2. The weight vectors have similarities in neighbor neurons, and the neurons that have fewer similarities with the weight vectors are located further away on the map [20]. Thus, the similarity of the classes is visualized by the distance of the position vectors on the map. In the classification of elastic waves, amplitudes of noises are assumed to be lower in comparison with diffraction waves wherein amplitudes are lower than straight propagation waves. Moreover, the used weight vectors are related with the size of the amplitudes because the used weight vectors were computed from the measured waveform. It is supposed that the location of the high S/N class, wherein straight propagations belong, is closer to the location of the low S/N class, wherein diffraction waves belong, in comparison with the location of the noise class. According to Figure 9, it is confirmed that visualized classes are in the expected location.

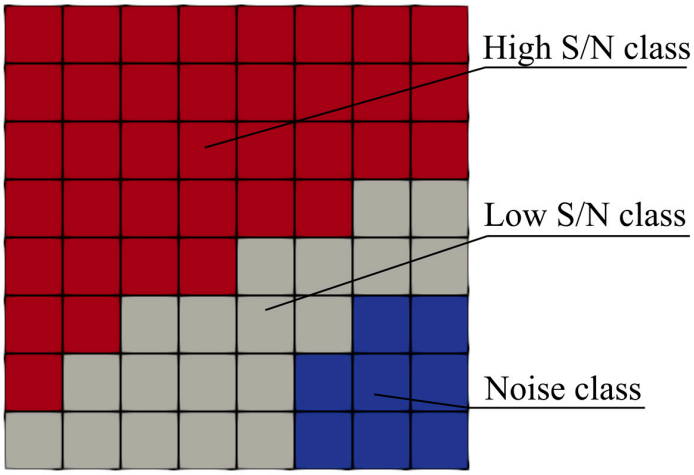

Figure 9. Results of SOM using artificial AEs measured at S1, S4, S9, and S12.

Three-dimensional vectors computed from each measured wave are applied to the map to conduct the classification. It should be noted that the winning neuron is computed by Equation (5) using the measured waveform, and the class of the winning neuron implies the class of the waveform. The results of the classifications for the measured waves at each sensor are shown in Figure 10. According to Figure 10, high S/N signals are measured at each sensor, but particularly few high S/N signals are acquired at S3 and S4. Since the occurrence of a large amount of diffraction around the defects is expected, S3 and S4 have potential for measuring the larger numbers of diffraction waves in comparison with the number of straight propagation waves. Therefore, it is confirmed that the results of the classification approximate the above prediction. Furthermore, it is expected that the map performs the classification of elastic waves the same as the expected performances. In addition, it should be noted that the performance of the map used for classification will be confirmed if artificial AE arrivals are obtained from the waveform belonging to the high S/N class and the detected arrival times contribute to an improvement of the accuracies of the AE source localizations.

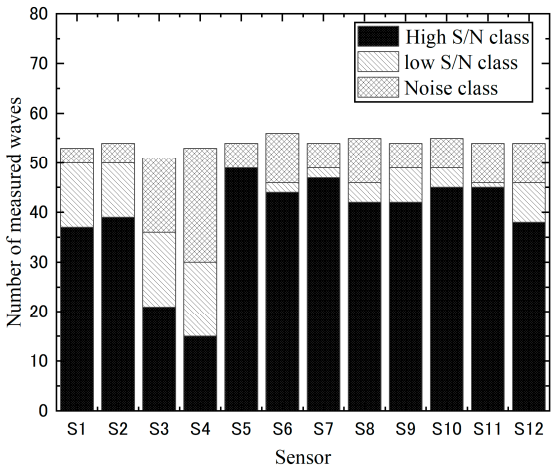

Figure 10. Results of the classification in each sensor.

5.2. Results of AE Source Localizations

In order to validate the performance of AE source localizations with the classified waves, arrival times were detected from the classified waves which are expected to propagate as straight lines, and the detected arrival times are applied to the source localizations, which are the TDOA method and ray tracing. Moreover, the performance of the classification of the AE source localizations conducted on heterogeneous velocity distributions is

discussed through comparisons with source localizations using all of the measured waves. It should be noted that these models assume the propagation velocity is 5400 m/s, referring to the results of the source localization conducted on an aluminum plate [22].

The results of the TDOA method are shown in Figure 11. Although the localized sources shown in Figure 11a have low accuracies, the localized sources shown in Figure 11b approximate the locations of PLB points. Figure 11a confirms that the diffraction waves contribute to source-localization errors because the algorithm of the TDOA method assumes ray paths to be straight propagations. Thus, the used waveforms in Figure 11b are possibly propagated as straight, and it is demonstrated that the classification improves the results of the TDOA method in the heterogeneous velocity distributions. Furthermore, the classified waves in the source localization based on ray tracing perform as well as in the TDOA method. The sources localized by ray tracing are shown in Figure 12. It is noted that the source is chosen from candidates set with the interval of 20 mm. In the ray-tracing algorithm, diffraction waves are considered on the basis of approximated heterogeneities by the cells in models. The ray tracing is conducted on the homogenous model and the localization errors are generated in Figure 12a. However, the accuracy of the localized sources is reformed in Figure 12b, and it implies that use of ray tracing for the source does not require the approximation of velocity distributions in the model if the straight propagation waves are classified.

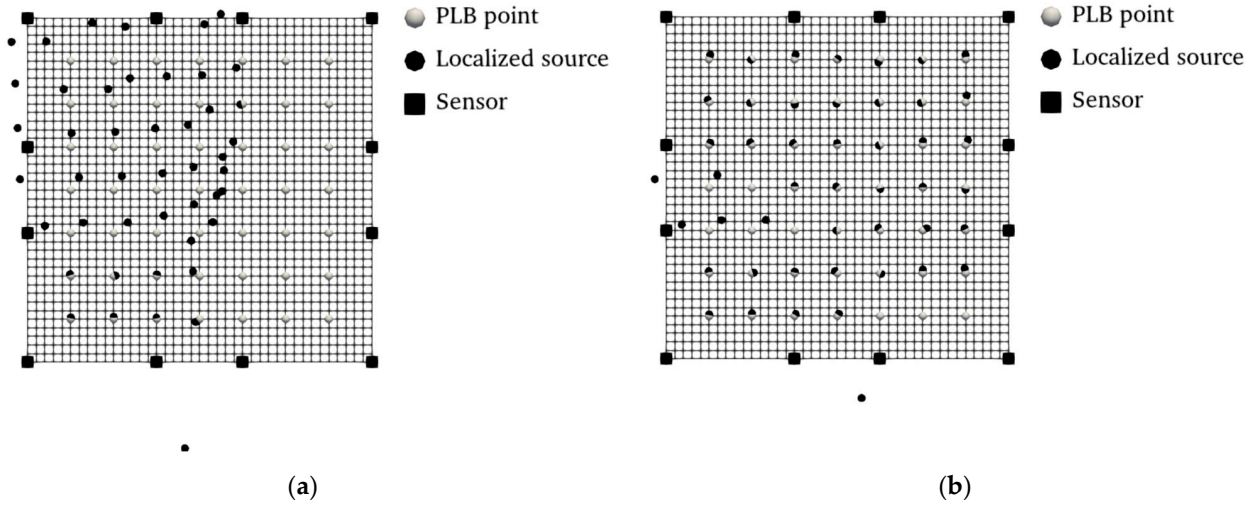

Figure 11. Results of TDOM method in the heterogeneous elastic velocity distributions: (**a**) non-classification; (**b**) the application of the classification.

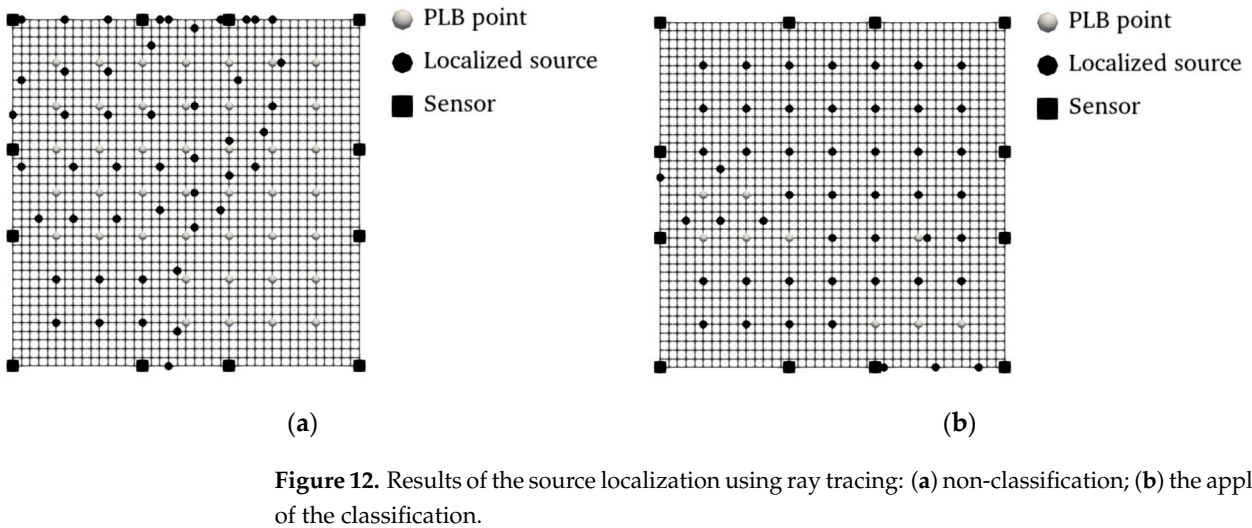

Figure 12. Results of the source localization using ray tracing: (**a**) non-classification; (**b**) the application of the classification.

The results of the source localizations using the classified waves are listed in Table 2. The visualized events imply the number of sources localized in Figures 11b and 12b. In Table 2, the visualized events of the TDOA method exclude two sources that had huge localization errors due to the divergence of the least squares method. Hence, although the number of the sources localized by ray tracing is the same as the number of PLB tests, the number of the sources localized by the TDOA method is smaller in comparison with the number of PLB tests. Moreover, the errors regard Euclidean distance, which is from a PLB point to a localized source. Furthermore, the average and the maximum of errors are computed on the basis of visualized events. In the visualized events, the average errors of TDOA are the approximated results of ray tracing. However, the TDOA method generates a larger maximum error in comparison with the application of ray tracing. It should be noted that the effect of the arrival-time detection error in source localizations with classified waves is expected to be larger in comparison with the effect of diffractions [22]. Although the localized sources have the potential to be visualized out of the analytical model in the TDOA algorithm if the detection errors of arrival times are large, the sources are localized in the analytical model if the ray tracing is applied to a source localization since localized sources are obtained as candidates. Therefore, it is confirmed that ray tracing prevents larger localization errors than the use of the TDOA method. However, according to the computational times which are user CPU times using an i7-8550U processor in a single thread, the TDOA method spends less than 1.0 s. Moreover, ray tracing localizes sources in 801 s. It is confirmed that the TDOA method does not require huge computational times in comparison with the use of ray tracing.

Table 2. Results of the source localizations with the classified waves.

Source Localization	Visualized Events	Average Errors (mm)	Maximum Errors (mm)	Computational Time (s)
TDOA	47	15	200	0.011
Ray tracing	49	15	110	801

6. Discussion

In this model test, limited waves measured at the vertexes of the models were applied to the SOM. According to the results of the source localizations, it is confirmed that the obtained map performs classification of the straight propagation waves and improves the AE source localizations in the heterogeneous velocity distributions. Hence, the used measured waves are appropriate for the classification. It is noted that this selection of measured waves assumes that the source localizations are conducted in materials that were locally damaged. If waves are measured at the vertexes of complex structures, measured diffraction waves are increased. According to the SOM algorithm, having a large number of diffraction waves contributes to expanding the size of the low S/N class, and it is expected that classified straight propagations are decreased because of a reduction of the high S/N class. Hence, it implies that localized sources are decreased since few straight propagations are classified.

According to the comparison of the source localizations, ray tracing visualizes a larger number of sources than the TDOA method. In this model test, the least squares method is applied to the TDOA method and the location of a source error is iteratively corrected. If detection errors of arrival times are large, a source is firstly localized out of the analytical model. Furthermore, a coefficient matrix used in the least squares method computes the determinant of approximated 0 if a localized source firstly includes a large error. If the determinant is 0, the result of the TDOA method is the divergence. Furthermore, the particular combination of used sensor locations contributes to the computation of the determinant of 0. However, the application of ray tracing is expected to visualize all sources since the computation does not require a coefficient matrix. Therefore, it is noteworthy that the TDOA method has potential to visualize a smaller number of sources in comparison with the number of sources localized by ray tracing if the classified waves

are applied. Moreover, the maximum localization error generated by the TDOA method is larger than the error of the localization based on the ray tracing. Although the averages of source localization errors are approximated in the two localizations, the number of sources localized by ray tracing includes two of the sources which are not localized by the TDOA method. It should be noted that the arrival-time detection errors generate the determinant of approximated 0 in the coefficient matrix, and this reason is why two of the sources are not localized by the TDOA method. In the localizations based on ray tracing, two of the sources are expected to have larger errors than the average because of the arrival-time detection errors. Therefore, in the application of the classified waves, it is expected that the sources localized by ray tracing are more accurate than the accuracy in the TDOA method. It should be noted that this model of ray tracing set the intervals of the candidates at 20 mm. Moreover, Kobayashi et al. localized sources in which the average error was approximated at half of the interval of the candidates [32]. Owing to the average error of 15 mm in the TDOA method, it is expected that the 20 mm interval of the candidates is sufficient in the localization based on ray tracing using classified waves. Consequently, the localization based on ray tracing is appropriate in the application of classified waves if the interval of 20 mm is used.

Although ray tracing more accurately localizes sources than the TDOA method, the computational times of ray tracing are huge. According to the ray-tracing algorithm [21], all possible ray paths are computed on the basis of the candidate points and an approximated velocity distribution to approximate a ray path; a first travel time is then determined as an approximated ray path. In the application of classified waves, approximated ray paths are not required in the source localization because straight propagation waves are classified. Thus, the computation time is expected to be optimized.

7. Conclusions

The application of classification based on the SOM has potential for classifying straight propagation waves. Thus, conventional AE source localizations are expected to perform in heterogeneous elastic wave velocity distributions if classified waves are applied. Although the TDOA method is expected to have reduced visualized sources because the classified waves have the potential to compute the determinant of 0, the application of ray tracing localizes sources with lower accuracy in comparison with sources localized by the TDOA method if the interval of the candidates is too low. In order to validate the performance of the source localizations with the classified waves, the classified waves were applied to the TDOA method and the ray tracing in this study. Moreover, the model tests based on PLB were conducted to validate the performance of the source localizations. Furthermore, the AEs used in the SOM were validated to evaluate the localization accuracy since the results of the SOM depend on the selected AEs. The conclusions obtained from the model test are listed as follows:

- Selected waves measured at the vertex of the specimen were applied to the SOM. According to the results of the AE source localizations assuming homogeneous velocity distributions, the accuracy of localized sources in heterogeneous velocity distributions was improved by the use of the waves classified on the basis of the map. Therefore, it is confirmed that this selection of waves for the SOM is appropriate in the classification of elastic waves. It should be noted that this selection of the measured waves assumes that the source localizations are conducted in materials that were locally damaged.
- In the particular location of sensors, AE source localization based on ray tracing localizes a larger number of sources in comparison with the computation of the TDOA method because of the divergence in the least squares method used in the TDOA method. Moreover, the TDOA method generates maximum errors in the comparison of the source localizations. Therefore, it is confirmed that the source localization based on ray tracing is appropriate in the application of classified waves if the interval of the candidates is 20 mm.

- The computational times of ray tracing are huge, and the optimization of the computation time is required. In the application of classified waves, approximated ray paths are not required in the source localization because straight propagation waves are classified. Thus, the computation time is expected to be optimized.

In the use of machine learning for source localization, unsupervised learning methods should be applied for versatility because the characteristics of AE signals depend on the sources, the propagated materials, and the measurement system. However, supervised learning methods have been applied to the localizations for NDT [33–35]. In future works, the classification of elastic waves based on the SOM are going to be validated in comparison with supervised learning methods to show its superiority.

Author Contributions: Conceptualization, K.N.; methodology, K.N.; software, K.N.; validation, K.N.; formal analysis, K.N.; investigation, K.N., Y.K., K.O. and S.S.; resources, Y.K. and K.O.; data curation, K.N.; writing—original draft preparation, K.N.; writing—review and editing, Y.K., K.O. and S.S.; visualization, K.N. All authors have read and agreed to the published version of the manuscript.

Funding: This research received no external funding.

Institutional Review Board Statement: Not applicable.

Informed Consent Statement: Not applicable.

Data Availability Statement: Not applicable.

Conflicts of Interest: The authors declare no conflict of interest.

References

1. Yun, H.D.; Choi, W.C.; Seo, S.Y. Acoustic emission activities and damage evaluation of reinforced concrete beams strengthened with CFRP sheets. *NDT E Int.* **2010**, *43*, 615–628. [CrossRef]
2. Ciampa, F.; Meo, M. A new algorithm for acoustic emission localization and flexural group velocity determination in anisotropic structures. *Compos. Part A Appl. Sci. Manuf.* **2010**, *41*, 1777–1786. [CrossRef]
3. Kobayashi, Y.; Shiotani, T. *Innovative AE and NDT Techniques for On-Site Measurement of Concrete and Masonry Structures: State-of-the-Art Report of the RILEM Technical Committee 239-MCM*, 1st ed.; Ohtsu, M., Ed.; Springer: Dordrecht, The Netherlands, 2016; pp. 47–68.
4. Huang, J.; Qin, C.Z.; Niu, Y.; Li, R.; Song, Z.; Wang, X. A method for monitoring acoustic emissions in geological media under coupled 3-D stress and fluid flow. *J. Pet. Sci. Eng.* **2022**, *211*, 110227. [CrossRef]
5. Li, X.; Lin, W.; Mao, W.; Koseki, J. Acoustic emission source location of saturated dense coral sand in triaxial compression tests. In Proceedings of the 8th Japan-China Geotechnical Symposium, Kyoto, Japan, 14–15 March 2020.
6. Mao, W.; Goto, S.; Towhata, I. A study on particle breakage behavior during pile penetration process using acoustic emission source location. *Geosci. Front.* **2020**, *11*, 413–427. [CrossRef]
7. Carabelli, E.; Federici, P.; Graziano, F.; Rondena, E.; Zaninetti, A. Location of ae sources in the rock foundation of the passante dam. *Eng. Fract. Mech.* **1990**, *35*, 599–606. [CrossRef]
8. Manuello, A.; Gianni, N.; Carpinteri, A. AE monitoring of a concrete arch road tunnel: Damage evolution and localization. *Eng. Fract. Mech.* **2019**, *210*, 279–287. [CrossRef]
9. Kundu, T. Acoustic source localization. *Ultrasonics* **2014**, *54*, 25–38. [CrossRef]
10. Kawasaki, Y.; Ueda, K.; Izuno, K. AE source location of debonding steel-rod inserted and adhered inside rubber. *Constr. Build. Mater.* **2021**, *279*, 122383. [CrossRef]
11. Shiotani, T.; Osawa, S.; Kobayashi, Y.; Momoki, S. Application of 3D AE tomography for triaxial tests of rocky specimens. In Proceedings of the 31st Conference of the European Working Group on Acoustic Emission, Dresden, Germany, 3–5 September 2014.
12. Dong, L.; Tao, Q.; Hu, Q.; Deng, S.; Chen, Y.; Luo, Q.; Zhang, X. Acoustic emission source location method and experimental verification for structures containing unknown empty areas. *Int. J. Min. Sci. Technol.* **2022**, *32*, 487–497. [CrossRef]
13. Jones, M.R.; Rogers, T.J.; Worden, K.; Cross, E.J. A Bayesian methodology for localising acoustic emission sources in complex structures. *Mech. Syst. Signal Process.* **2022**, *15*, 108143. [CrossRef]
14. Lei, X.; Masuda, K.; Nishizawa, O.; Jouniaux, L.; Liu, L.; Ma, W.; Satoh, T.; Kusunose, K. Detailed analysis of acoustic emission activity during catastrophic fracture of faults in rock. *J. Struct. Geol.* **2004**, *26*, 247–258. [CrossRef]
15. Townend, E.; Thomapson, B.D.; Benson, P.M.; Meredith, P.G.; Baud, P.; Young, R.P. Imaging compaction band propagation in Diemelstadt sandstone using acoustic emission locations. *Geophys. Res. Lett.* **2008**, *35*, L15301. [CrossRef]
16. Baer, M.; Kradolfer, U. An automatic phase picker for local and teleseismic events. *Bull. Seismol. Soc. Am.* **1987**, *77*, 1437–1445. [CrossRef]

17. Lokajíček, T.; Klíma, K. A first arrival identification system of acoustic emission (AE) signals by means of a high-order statistics approach. *Meas. Sci. Technol.* **2006**, *17*, 2461. [CrossRef]
18. Takanami, T.; Kitagawa, G. A new efficient procedure for the estimation of onset times of seismic waves. *J. Phys. Earth* **1988**, *36*, 267–290. [CrossRef]
19. Sedlak, P.; Hirose, Y.; Enoki, M. Acoustic emission localization in thin multi-layer plates using first-arrival determination. *Mech. Syst. Signal Process.* **2013**, *36*, 636–649. [CrossRef]
20. Kohonen, T. Essentials of the self-organizing map. *Neural Netw.* **2013**, *37*, 52–65. [CrossRef]
21. Kobayashi, Y. Mesh-independent ray-trace algorithm for concrete structure. *Constr. Build. Mater.* **2013**, *48*, 1309–1317. [CrossRef]
22. Nakamura, K.; Kobayashi, Y.; Oda, K.; Shigemura, S. Classification of Elastic Wave for Non-Destructive Inspections Based on Self-Organizing Map. *Sustainability* **2023**, *15*, 4846. [CrossRef]
23. Tian, H.; Qiang, P.; Xiandong, L.; Yingchun, S. AE beamforming method for damage inspection of aircraft structures. *Procedia Eng.* **2011**, *17*, 297–302. [CrossRef]
24. Xiao, D.; He, T.; Pan, Q.; Liu, X.; Wang, J.; Shan, Y. A novel acoustic emission beamforming method with two uniform linear arrays on plate-like structures. *Ultrasonics* **2014**, *54*, 737–745. [CrossRef]
25. Mirgal, P.; Pal, J.; Banerjee, S. Online acoustic emission source localization in concrete structures using iterative and evolutionary algorithms. *Ultrasonics* **2020**, *108*, 106211. [CrossRef]
26. Li, X.; Naqi, A.; Maqsood, Z.; Koseki, J. Verification of 3D AE Source Location Technique in Triaxial Compression Tests Using Pencil Lead Break Sources on a Cylindrical Metal Specimen. *Appl. Sci.* **2022**, *12*, 1603. [CrossRef]
27. Rasti, J.; Monadjemi, A.; Vafaei, A. Color reduction using a multi-stage Kohonen Self-Organizing Map with redundant features. *Expert Syst. Appl.* **2011**, *38*, 13188–13197. [CrossRef]
28. Godin, N.; Huguet, S.; Gaertner, R. Integration of the Kohonen's self-organising map and k-means algorithm for the segmentation of the AE data collected during tensile tests on cross-ply composite. *NDT E Int.* **2005**, *38*, 299–309. [CrossRef]
29. Nakamura, K.; Kobayashi, Y.; Oda, K.; Shigemura, S.; Ikebata, K. Validation of elastic wave arrival detection method based on use of sparse matrix computation. *IOP Conf. Ser. Mater. Sci. Eng.* **2022**, *1242*, 012025. [CrossRef]
30. Physical Acoustics Corporation. *AEwin Software User's Manual, Express-8 AE System*; Physical Acoustics Corporation: West Windsor, NJ, USA, 2014.
31. Bhuiyan, M.A.H.; Karmaker, S.C.; Saha, B.B. Nexus between potentially toxic elements' accumulation and seasonal/anthropogenic influences on mangrove sediments and ecological risk in Sundarbans, Bangladesh: An approach from GIS, self-organizing map, conditional inference tree and random forest models. *Environ. Pollut.* **2022**, *309*, 119765. [CrossRef]
32. Kobayashi, Y.; Oda, K.; Nakamura, K. A Source Localization Technique Based on a Ray-Trace Technique with Optimized Resolution and Limited Computational Costs. *Proceedings* **2018**, *2*, 477. [CrossRef]
33. Chu, H.; Wang, W.; Deng, L. Tiny-Crack-Net: A multiscale feature fusion network with attention mechanisms for segmentation of tiny cracks. *Comput.-Aided Civ. Infrastruct. Eng.* **2022**, *37*, 1914–1931.
34. Sampath, S.; Jang, J.; Sohn, H. Ultrasonic Lamb wave mixing based fatigue crack detection using a deep learning model and higher-order spectral analysis. *Int. J. Fatigue* **2022**, *163*, 107028.
35. Wu, J.; Xu, X.; Liu, C.; Deng, C.; Shao, X. Lamb wave-based damage detection of composite structures using deep convolutional neural network and continuous wavelet transform. *Compos. Struct.* **2021**, *276*, 114590.